



## Article

# Comparative Studies between Frequency Domain Analysis and Time Domain Analysis on Free-Field One-Dimensional Shear Wave Propagation

Sun-Hoon Kim <sup>1,\*</sup>  and Kwang-Jin Kim <sup>2</sup><sup>1</sup> Department of Civil and Environmental Engineering, U1 University, Yeongdong-kun 29131, Republic of Korea<sup>2</sup> Comtec Research, Seocho-ku, Seoul 06650, Republic of Korea; info@comtecresearch.co.kr

\* Correspondence: kimsh@yd.ac.kr

**Abstract:** In Korea, the underground silo structure for low- and intermediate-level radioactive waste disposal facilities has been constructed and operated since 2014. Large-scale earthquakes occurred in 2016 and 2017, respectively, in Gyeongju and Pohang areas near the underground silo structures, and interest in the stability of the underground silo increased significantly. In this paper, one-dimensional free-field analyses have been carried out before the three-dimensional silo dynamic analyses subjected to earthquake loadings. As an additional study, a new form of the finite element equilibrium equation is derived in terms of relative motions, which is essentially the same equation expressed in terms of total motions where the base shear force is applied to the earthquake load. The accuracy of conventional finite element solutions is evaluated by directly comparing them with closed-form solutions by frequency domain analysis such as SHAKE91.

**Keywords:** earthquake; free-field analysis; frequency domain analysis; time domain analysis; finite element analysis; shear wave propagation



**Citation:** Kim, S.-H.; Kim, K.-J. Comparative Studies between Frequency Domain Analysis and Time Domain Analysis on Free-Field One-Dimensional Shear Wave Propagation. *Appl. Mech.* **2024**, *5*, 141–161. <https://doi.org/10.3390/applmech5010009>

Received: 16 January 2024

Revised: 23 February 2024

Accepted: 25 February 2024

Published: 29 February 2024



**Copyright:** © 2024 by the authors. Licensee MDPI, Basel, Switzerland. This article is an open access article distributed under the terms and conditions of the Creative Commons Attribution (CC BY) license (<https://creativecommons.org/licenses/by/4.0/>).

## 1. Introduction

The underground disposal program for low- and intermediate-level radioactive waste was commissioned in the late 1970s. From the beginning, the design criterion was a stratified disposal, and its safety depends on natural and engineering barriers. The treatment system has to isolate the waste for hundreds of years. During this period, the radioactive toxicity of the waste is greatly reduced [1]. Radioactive wastes include spent nuclear fuels, which have been used for fuels in nuclear power stations, low- and intermediate-level wastes (work clothes, globes, and replaced parts), which have been used by workers in the controlled area in a nuclear power station, and radioisotope wastes, which have been generated from hospitals, research institutions, and industries. They should be managed safely for a certain period according to the relevant laws and regulations [2,3].

In Korea, the Wolsong Low and Intermediate Level Radioactive Waste Disposal Center (WLDC) has been under construction with a total capacity of 800,000 drums. The first phase of the construction, which is the underground silo for LILW (Low- and Intermediate-Level radioactive Waste) disposal facilities with a 100,000 drum capacity, was completed in 2014 (see Figure 1) [2]. The facility in the first phase was constructed underground, 130 m below sea level consisting of six silos, 23.6 m in diameter and 50 m in height (see Figure 2) [3,4]. The engineered barrier system of the underground silo consisted of waste packages, disposal containers, backfills, and a concrete silo. Many studies have been conducted and published to verify the safety assessment since the facility was completed [5–7].

Although Korea has been recognized as a safe country for earthquakes, relatively large-scale earthquakes occurred in 2016 and 2017, respectively. The 2016 Gyeongju Earthquake (local magnitude (ML) of 5.8) and the 2017 Pohang Earthquake (ML of 5.4) were reported to have caused a lot of damage to many buildings and facilities in the surrounding

area [8,9]. These earthquakes occurred in the area adjacent to WLDC, and the distances from the epicenter were 26 and 46 km, respectively. Therefore, interest in the stability of the underground silo increased significantly [4,10,11].



Figure 1. The layout of LILW disposal facilities in Wolsong.

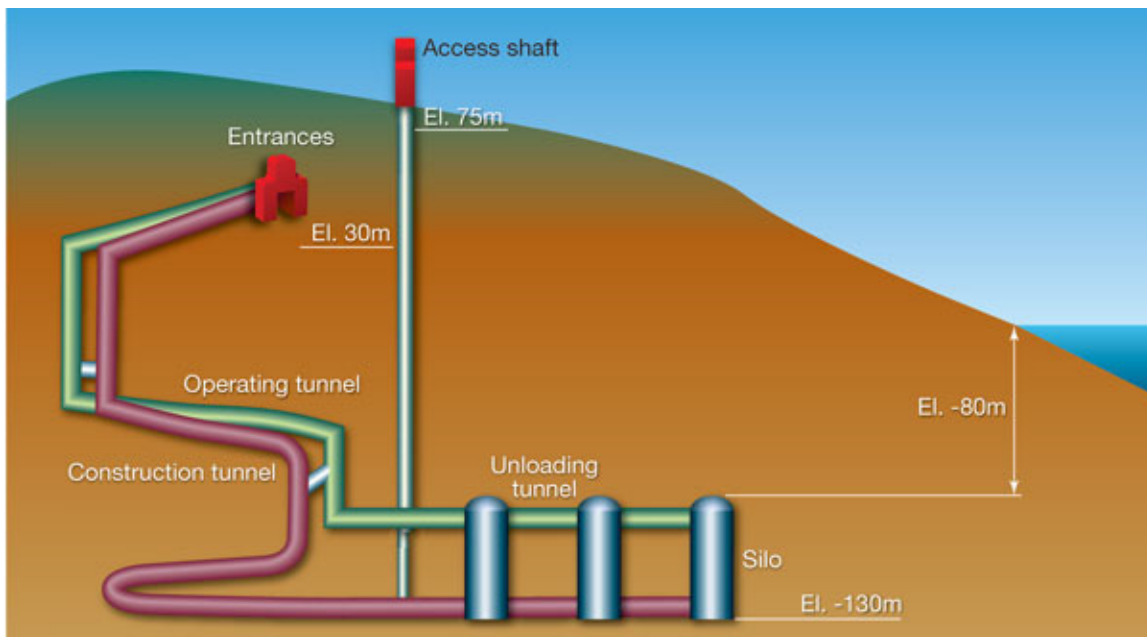


Figure 2. View of underground construction of LILW disposal facilities in Wolsong.

Since the underground silo structure has been used for many purposes, various studies have been published on earthquake responses as well as structural safety of underground silos in many countries around the world. In particular, many research results have been published on the underground silo as a radioactive waste repository [1,12], the definition of the underground silo as a structure [13], the effect of friction with walls or floors [14,15], and the seismic vulnerability problem of all containers [16,17].

However, unfortunately, there is little research on the seismic analysis of rocks around underground silos for LILW disposal facilities [12,18].

Silo structural analyses consisted of the following three parts:

- Stress distribution in rocks around underground silo, published in Ref. [4].

The 2D axial symmetry and 3D finite element analyses were carried out under various ratios of in situ horizontal stress to vertical stress ( $K_0$ ).

- Silo concrete linings subjected to residual water pressure, published in Ref. [19].

The 2D axial symmetry and 3D finite element analyses were performed considering separation and slippage of interface joints between shotcrete and lining.

- The 3D silo dynamic analyses subjected to earthquake loads, in preparation.

The 1D frequency and time domain analyses were performed under free field. The 3D finite element analyses were conducted considering nonlinear interface joints and elasto-plastic surrounding rocks.

In this study, free-field one-dimensional analyses have been performed before the three-dimensional silo dynamic analyses considering the following:

- Closed-form solutions (SHAKE, SHAKE91, DEEPSOIL, etc.) in the frequency domain are available for one-dimensional shear wave propagation in the linearly viscous elastic system subjected to base accelerations.
- Numerical finite element solutions as the time domain analysis can be directly compared to such closed-form solutions in the free fields including the lateral boundary so that we can assess the accuracy of numerical solutions.

Five different computer programs are used for the comparative studies between frequency and time domain analyses as listed in Table 1.

**Table 1.** Computer programs used for the study.

Name	Analysis Method	Modulus and Damping	Ref.
SHAKE91	Frequency Domain (1D)	Strain Compatible Values	[20]
DEEPSOIL	Frequency Domain (1D)	Strain Compatible Values	[21]
SRAP-1D	Time Domain Modal (1D)	Compatible Values Based on Equivalent Uniform Strain	[22]
QUAD-4M	Time Domain FEM (2D)	Compatible Values Based on Equivalent Uniform Strain	[23]
SMAP-3D	Time Domain FEM (3D)	General Nonlinear Modulus Rayleigh Proportional Damping	[24]

In a parallel study to this paper, a new form of the finite element equilibrium equation, Equation (2), is derived in terms of relative motions, which is essentially the same equation as that expressed in terms of total motions, Equation (3), where the base shear force is applied for the earthquake load [18]. The accuracy of conventional finite element solutions, Equation (2) without constant (a), is evaluated by directly comparing them with closed-form solutions using a frequency domain analysis such as SHAKE91 [20].

## 2. Linear Frequency Domain Analysis

### 2.1. Main Algorithm of the Frequency Domain Analysis

Frequency domain analysis has been used for the solution of site responses subjected to vertically propagating shear waves as schematically shown in Figure 3. For such analysis, SHAKE [25] has been the most popular computer program because of its simplicity and practicality in using the program. Since SHAKE, more recent versions have been written to improve the user interface and to show graphical outputs such as SHAKE91 and SHAKE2000 [26].

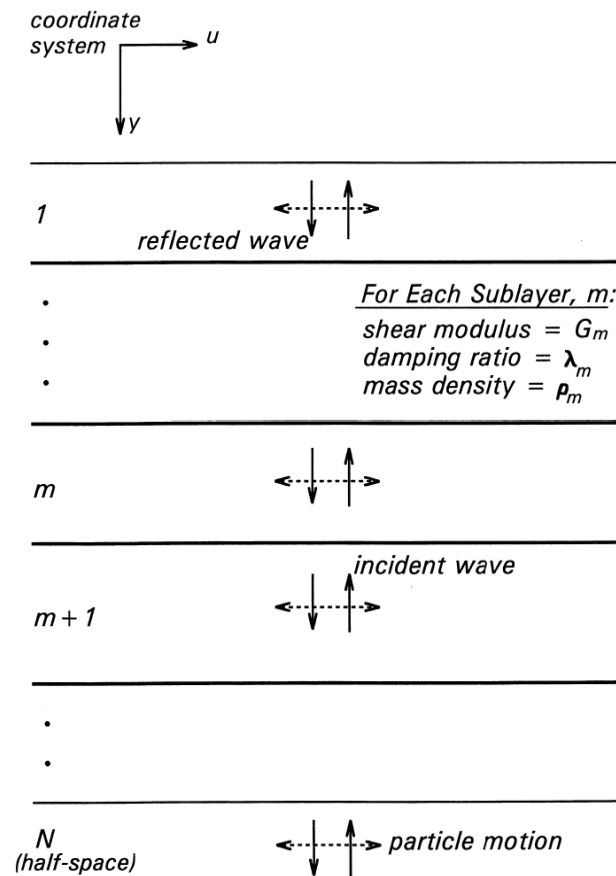


Figure 3. One-dimensional system over a uniform half-space.

The main characteristics of the wave motions in the horizontally layered system may be described such as in the following statements. In each layer, the horizontal particle motion consists of the upward incident wave and the downward reflected wave. On the interface between the adjacent layers, displacements and stresses are continuous. On the top surface, the amplitude of the incident wave is the same as that of the reflected wave since the shear stresses should be zero on such a free ground surface. Thus, the amplitude on the top surface is equal to twice the magnitude of the incident wave. On the bottom surface, the downward reflected wave is absorbed into the elastic half-space so that the upward incident wave will not be interrupted by the overlying soil deposit. It should be noted that such an upward incident wave is half of the magnitude of “outcrop bedrock motion” for the same reason as explained for the top ground surface.

The main algorithms of the frequency domain analysis may be described in the following way. For each harmonic motion, set up transfer functions for the incident and reflected waves in each layer and refer to SHAKE for the detailed derivation. These transfer functions represent the ratio of amplitudes in a layer to those at the top surface. The input object accelerations in the time domain are converted to the Fourier series form in the frequency domain using the Fast Fourier Transform (FFT) method. Amplitudes at any location in the layer can be found by using the Fourier series and transfer functions in the frequency domain and then responses in the time domain can be determined by inverting FFT.

### 2.2. Site Profile and Response Spectra for Input Earthquake

Figure 4 and Table 2 show the site profile and material properties used for all free-field analyses for both frequency domain and time domain analyses.

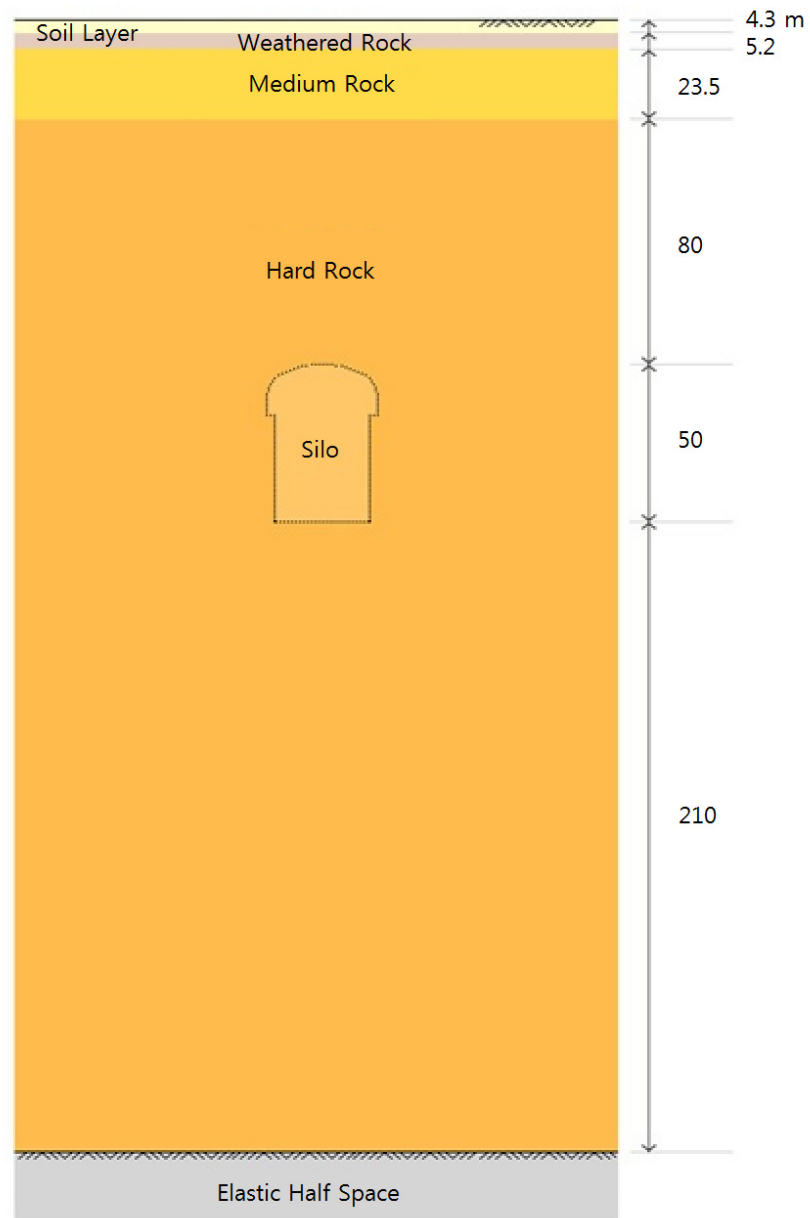
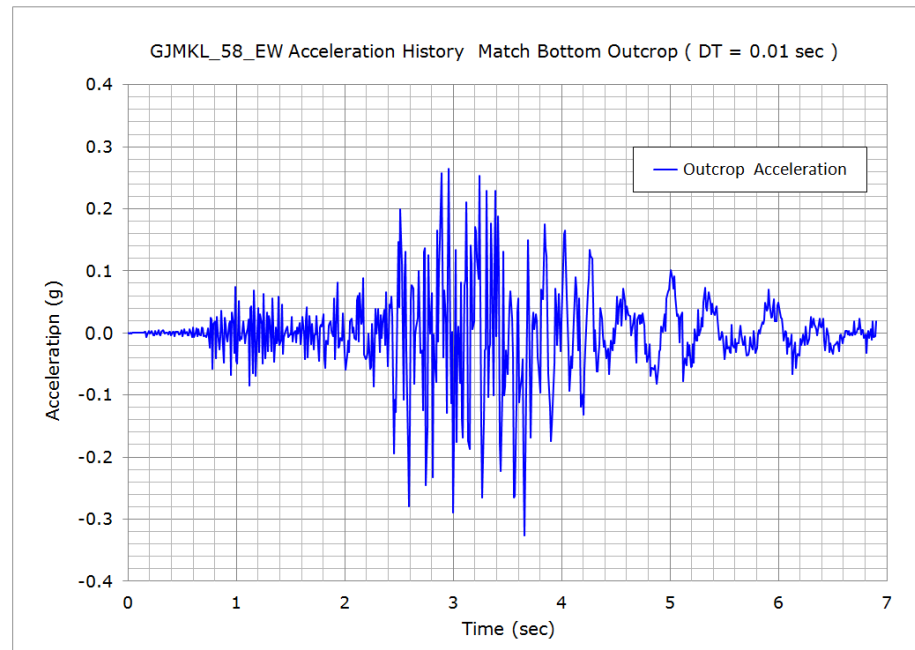


Figure 4. Site profile.

Table 2. Typical material properties of geomaterials.

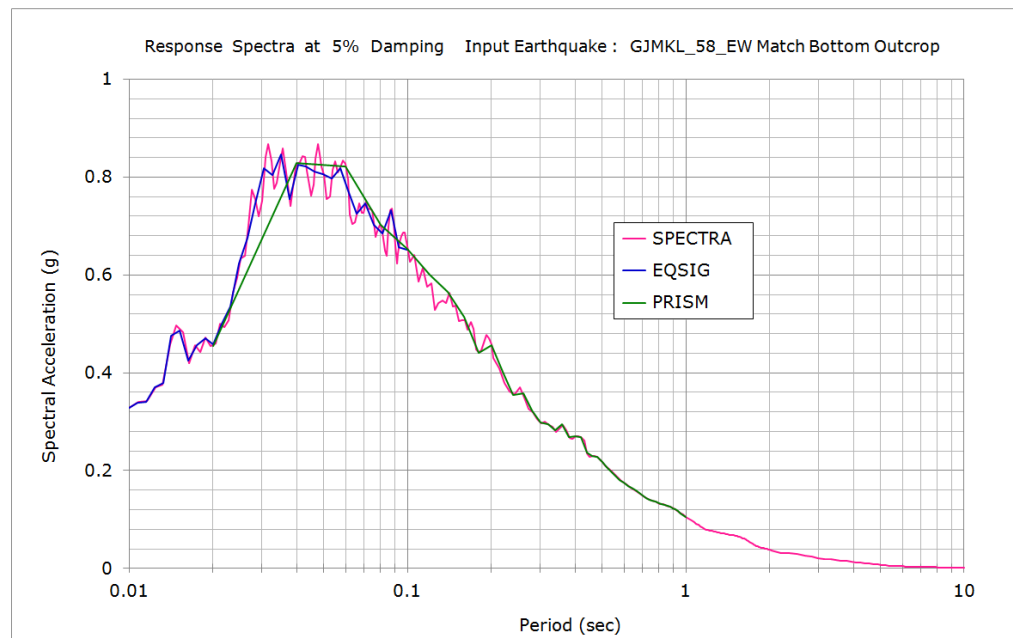
Ground Layer	Unit Weight (kN/m <sup>3</sup> )	Shear Wave Velocity (m/s)	Damping Ratio (%)
Soil Layer	18.63	495	5
Weathered Rock	20.59	792	5
Medium Rock	26.38	1500	3
Hard Rock	26.38	3477	2
Elastic Half Space	26.38	3607	1

Figure 5 shows input acceleration time history which has been used for the three-dimensional silo dynamic analyses as well as one-dimensional free-field analyses. This is the earthquake of local magnitude of ML = 5.8 recorded at the MKL station in Gyeongju Myeonggye-ri, Republic of Korea, on 12 September 2016 [9]. This input acceleration is applied as the outcrop motion at the base rock located 373 m below the ground surface.



**Figure 5.** Input acceleration time history.

The characteristics of this earthquake can be viewed by plotting the response spectra as shown in Figure 6. Spectral accelerations were computed by three different computer programs, SPECTRA [27], EQSIG [28], and PRISM [29]. They all show that absolute spectral accelerations are so high in periods between 0.03 and 0.06 s, indicating peak spectra values occurring at such high-frequency regions.



**Figure 6.** Response spectra for input earthquake.

Two computer programs (SHAKE91 [20] and DEEPSOIL version 7 [21]) are selected for the closed-form solutions in the frequency domain. Figure 7 shows the portion of the input user interface captured from the program DEEPSOIL.

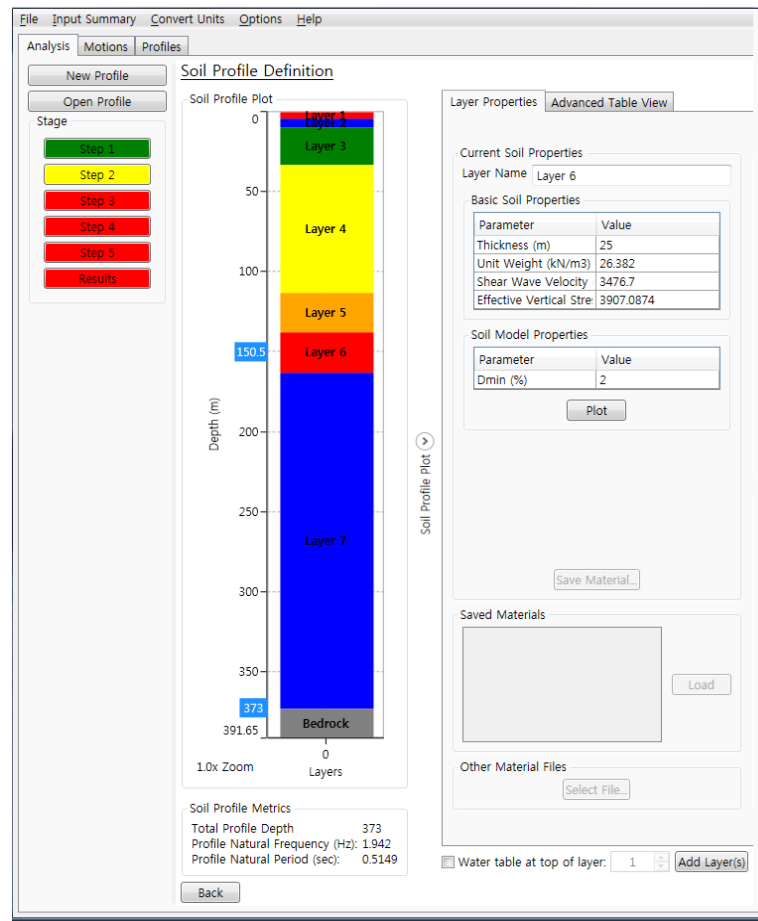


Figure 7. DEEPSOIL input user interface.

### 2.3. Analysis Results

Figure 8 shows the acceleration time histories on the ground surface which compare SHAKE91 to DEEPSOIL. Figure 9 shows the same comparison between  $t = 2$  and  $t = 4$  s, showing almost identical responses in the time where strong motions occur.

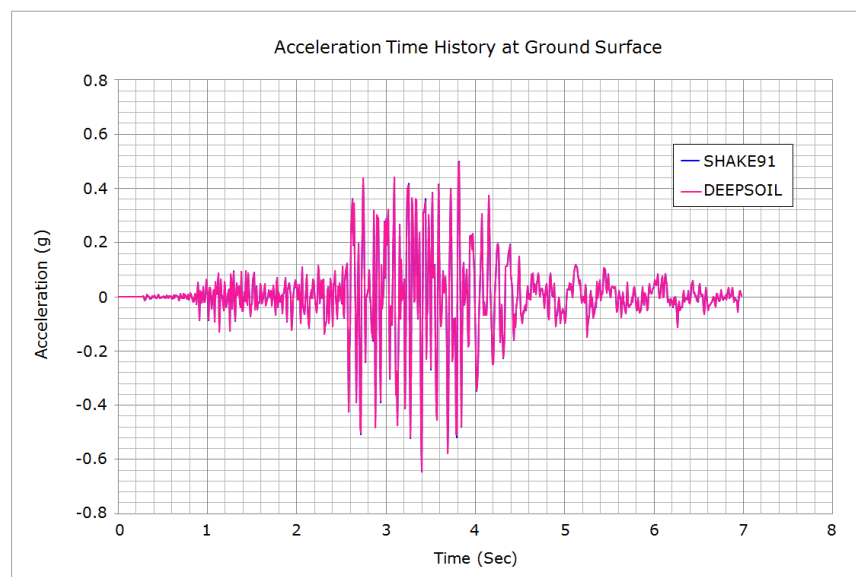
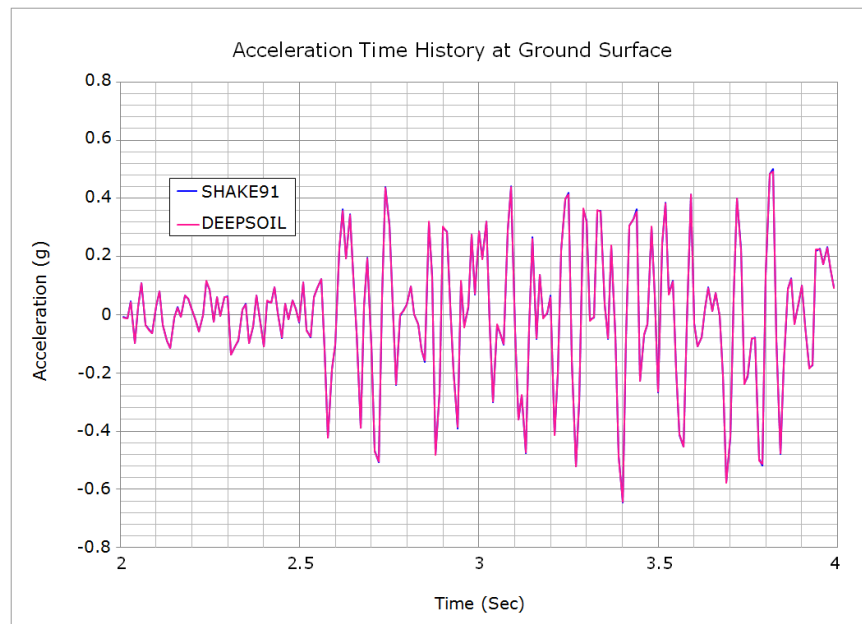
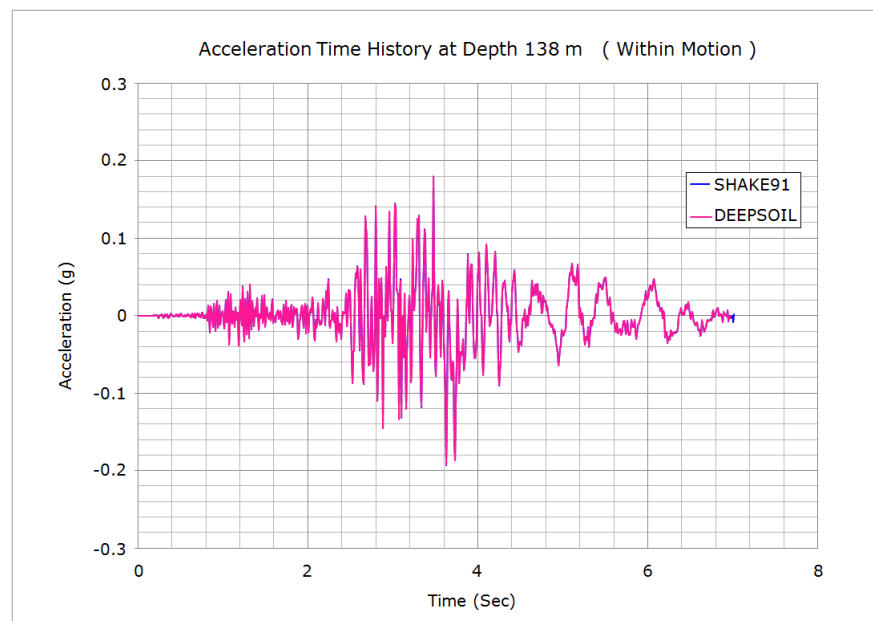


Figure 8. Acceleration time history on the ground surface which compare SHAKE91 to DEEPSOIL.



**Figure 9.** Acceleration history on the ground surface, between 2 and 4 s.

Figure 10 shows the acceleration time histories at a depth of 138 m which compare SHAKE91 to DEEPSOIL. Figure 11 shows the same comparison between  $t = 2$  and  $t = 4$  s, showing almost identical responses in the time when strong motions occur. Note that this depth corresponds to the location of the silo mid height as shown in Figure 4.



**Figure 10.** Acceleration time history at depth 138 m (within motion) which compare SHAKE91 to DEEPSOIL.

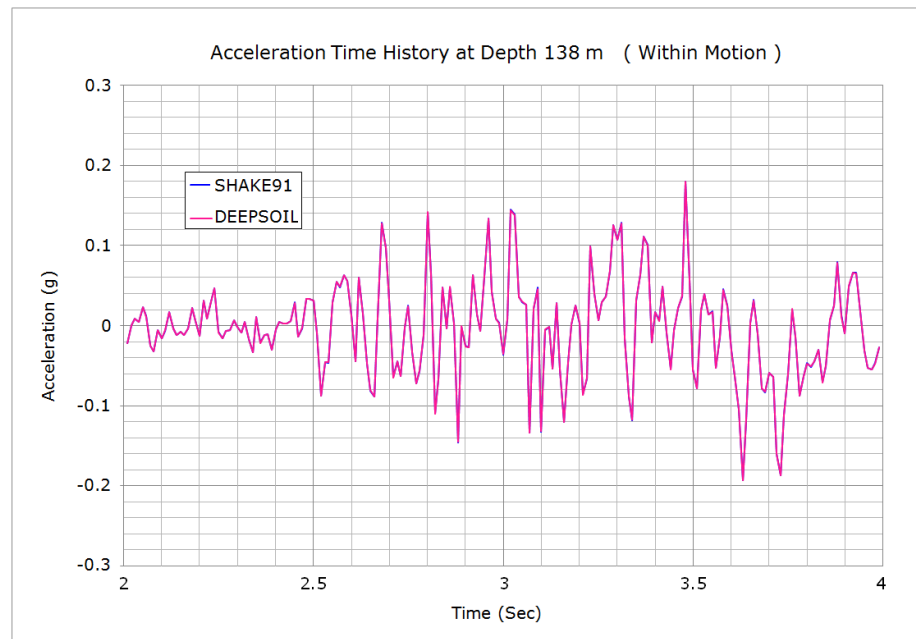


Figure 11. Acceleration history at depth 138 m, between 2 and 4 s.

### 3. Linear Time Domain Analysis

#### 3.1. Finite Element Formulations of Dynamic Equation

In the previous section, the frequency domain analysis solves the site responses based on wave equations with appropriate boundary conditions using the Fourier transformation method which converts input motions from the time domain to the frequency domain and then obtains responses in the time domain by inverse transformation.

Time domain analysis involves setting up the global dynamic equilibrium in a spatially discretized system and solving the equilibrium equation directly by the time marching schemes such as the Newmark method. The finite element analysis is the most popular and powerful method that has been used to obtain dynamic solutions in the time domain.

Finite element formulations of dynamic equations for linearly viscous elastic material subjected to base earthquake motions may be expressed in the following matrix form at time step  $n$ .

$$\mathbf{M} \ddot{\mathbf{u}}_n + \mathbf{D} \dot{\mathbf{u}}_n + \mathbf{K} \mathbf{u}_n = \mathbf{R}_n \tag{1}$$

when  $\mathbf{u}$  represents the relative displacement,

$$\mathbf{R}_n = -\mathbf{M} \cdot \mathbf{I} \cdot (\ddot{\mathbf{u}}_{gn} + a \cdot \dot{\mathbf{u}}_{gn}) \tag{2}$$

when  $\mathbf{u}$  represents the total displacement,

$$\mathbf{R}_n = \rho_r \cdot c_{sr} \cdot A_s \cdot \mathbf{J} \cdot \dot{\mathbf{u}}_{gn} \tag{3}$$

$$\mathbf{I}^T = \langle 1 \ 1 \ \dots \ 1 \ 1 \rangle$$

$$\mathbf{J}^T = \langle 0 \ 0 \ \dots \ 0 \ 1 \rangle$$

where

$\mathbf{M}, \mathbf{D}, \mathbf{K}$  are the mass, damping and stiffness matrices;

$\dot{\mathbf{u}}_{gn}, \ddot{\mathbf{u}}_{gn}$  are the earthquake outcrop velocity and acceleration at the bedrock;

$\rho_r, c_{sr}$  are the mass density and shear wave velocity at the bedrock;

$a$  is the Rayleigh mass proportional damping constant; and

$A_s$  is the tributary where the base shear is acting.

For the direct time integration of Equation (1), the Newmark constant average acceleration method, which is unconditionally stable, may be used.

$$\dot{\mathbf{u}}_n = \dot{\mathbf{u}}_{n-1} + (\ddot{\mathbf{u}}_{n-1} + \ddot{\mathbf{u}}_n) \cdot (\Delta t/2) \quad (4)$$

$$\mathbf{u}_n = \mathbf{u}_{n-1} + \dot{\mathbf{u}}_{n-1} \cdot \Delta t + (\ddot{\mathbf{u}}_{n-1} + \ddot{\mathbf{u}}_n) \cdot (\Delta t^2/4) \quad (5)$$

From Equations (4) and (5), we can obtain the following equations.

$$\ddot{\mathbf{u}}_n = (4/\Delta t^2) \cdot \mathbf{u}_n - \mathbf{A}_{n-1} \quad (6)$$

$$\dot{\mathbf{u}}_n = (2/\Delta t) \cdot \mathbf{u}_n - \mathbf{B}_{n-1} \quad (7)$$

Substituting Equations (6) and (7) into Equation (1), we obtain the following equation.

$$\bar{\mathbf{K}} \cdot \mathbf{u}_n = \bar{\mathbf{R}}_n \quad (8)$$

$$\bar{\mathbf{K}} = (4/\Delta t^2) \cdot \mathbf{M} + (2/\Delta t) \cdot \mathbf{D} + \mathbf{K} \quad (9)$$

$$\bar{\mathbf{R}}_n = \mathbf{R}_n + \mathbf{M} \cdot \mathbf{A}_{n-1} + \mathbf{D} \cdot \mathbf{B}_{n-1} \quad (10)$$

$$\mathbf{A}_{n-1} = 4 \cdot (\mathbf{u}_{n-1}/\Delta t^2 + \dot{\mathbf{u}}_{n-1}/\Delta t + \ddot{\mathbf{u}}_{n-1}/4) \quad (11)$$

$$\mathbf{B}_{n-1} = 2 \cdot (\mathbf{u}_{n-1}/\Delta t) + \dot{\mathbf{u}}_{n-1} \quad (12)$$

It is quite common practice to express the viscous damping by Rayleigh and Lindsay [30] which consists of mass and stiffness proportional terms at the element level.

$$\mathbf{D} = a \cdot \mathbf{M} + b \cdot \mathbf{K} \quad (13)$$

The energy loss associated with such viscous damping in Equation (13) is proportional to the velocity, which is also dependent on the frequency of the motion. The energy dissipation in soils, however, is independent on frequency even at very small strain levels based on experimental test data [31].

To mitigate such a frequency dependency in Rayleigh damping, the values of “a” and “b” in Equation (13) are expressed in terms of two target frequencies ( $\omega_1$  and  $\omega_i$ ) [32].

$$a = 2 \cdot \beta \cdot \omega_1 \cdot \omega_i / (\omega_1 + \omega_i) \quad (14)$$

$$b = 2 \cdot \beta / (\omega_1 + \omega_i) \quad (15)$$

where

$\omega_1$  is the fundamental natural circular frequency of the system

$\omega_i$  is the predominant circular frequency of the input earthquake motion;

$\beta$  is the critical damping ratio in an element.

### 3.2. Computer Programs for Free-Field Analysis

Three time domain computer programs are selected to perform the free-field analysis in the time domain, SRAP-1D, QUAD-4M, and SMAP-3D. SRAP-1D is a one-dimensional modal analysis program that is specific to the site response analysis subjected to earthquake motions. The original lumped mass solution listed in Ref. [22] is modified to include elastic half-space. QUAD-4M is a two-dimensional finite element program to evaluate the seismic response of soil structures [23]. SMAP-3D is the general-purpose three-dimensional finite element program developed by Comtec Research [24].

All three programs use the following schemes for free-field analyses:

- Lumped mass matrix as implicitly used by the frequency domain analysis.
- Transmitting boundary on the bottom of the finite element mesh for the elastic half-space.

- Two methods for applying external earthquake loadings [18].  
Method 1: Base accelerations to relative displacement fields as the conventional procedure which does not include Rayleigh mass damping constant (a), Equation (2).  
Method 2: Base shear to total displacement fields as earthquake load, Equation (3).
- The Newmark average acceleration method for the time integration.  
Figure 12 shows the cross-section of 3D finite element mesh modeled by SMAP-3D.

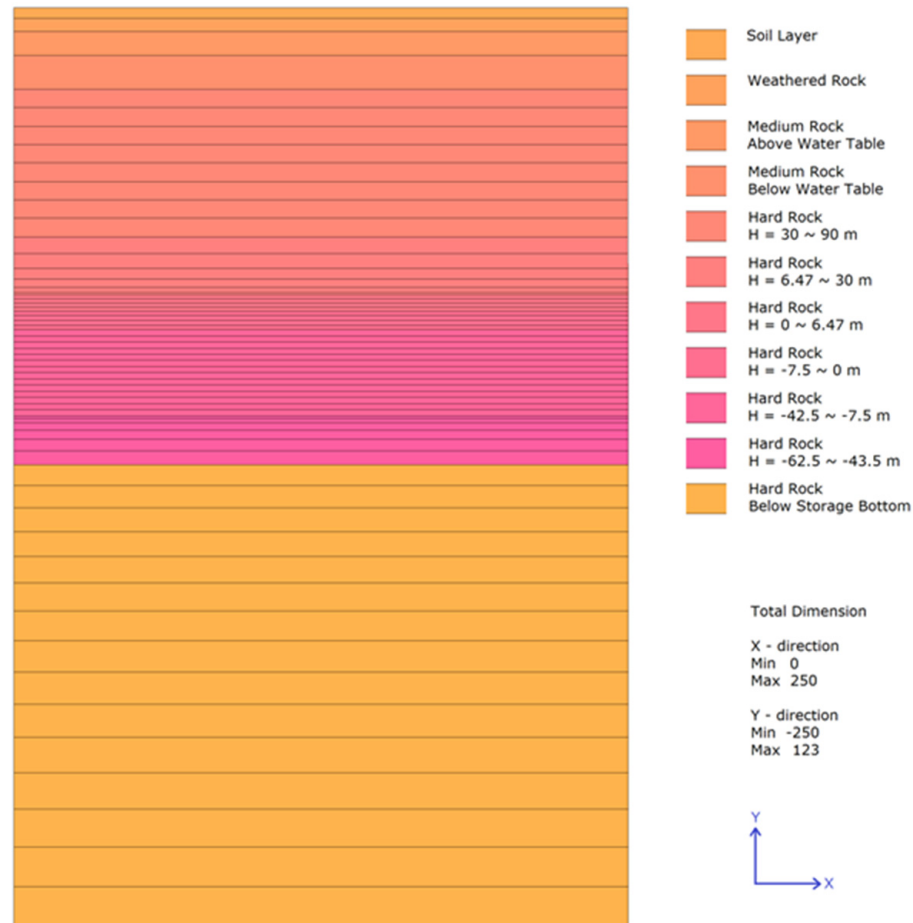


**Figure 12.** Finite element mesh used for 1D site response analysis.

### 3.3. Analysis Results

Figure 13 shows the acceleration time histories on the ground surface which compare the results of all three computer programs. Figure 14 shows the same comparison between  $t = 6$  and  $t = 8$  s, showing almost identical responses in the time where strong motions occur. It also shows that Method 1, the conventional procedure, produces almost the same results as Method 2. It should be noted that Method 1 would produce exactly the same results as Method 2 when we consider only stiffness proportional damping terms in Equation (13), as demonstrated in Ref. [18].

Figure 15 shows the acceleration time histories at a depth of 138 m which compare QUAD-4M to SMAP-3D. Figure 16 shows the same comparison between  $t = 6$  and  $t = 8$  s, showing almost identical responses in the time when strong motions occur. Note that this depth corresponds to the location of the silo mid height as shown in Figure 4.

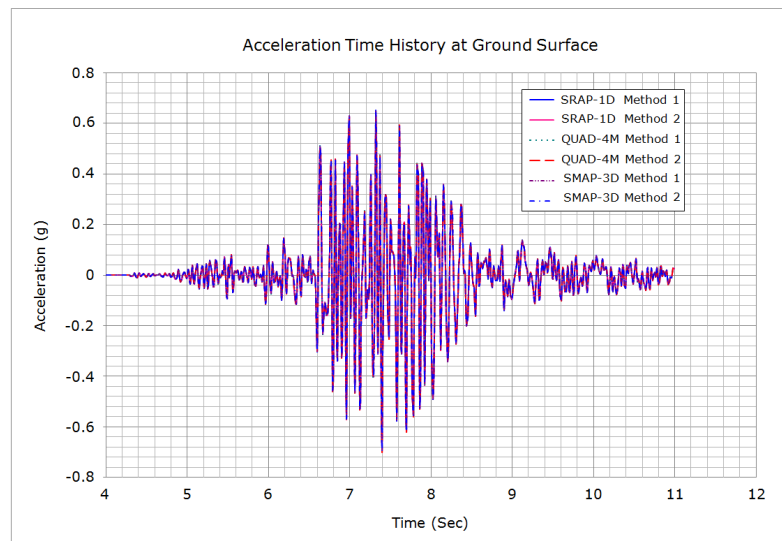


Figure 13. Acceleration time history on the ground surface, the results of all three computer programs.

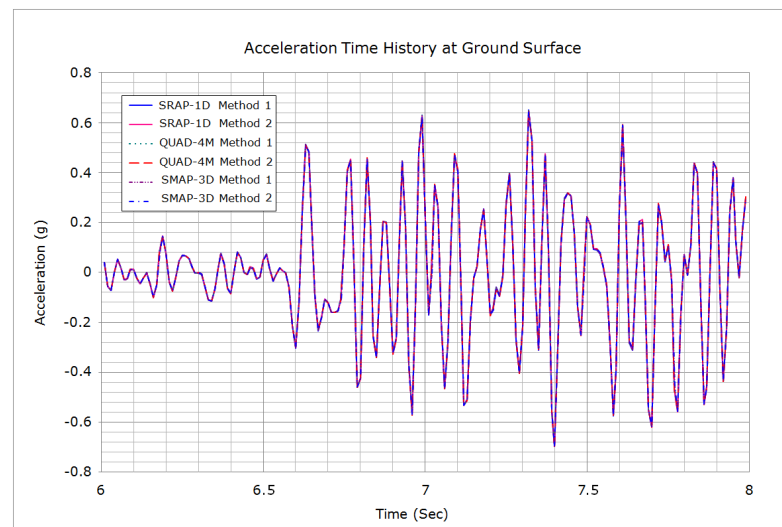


Figure 14. Acceleration history on the ground surface, between 6 and 8 s.

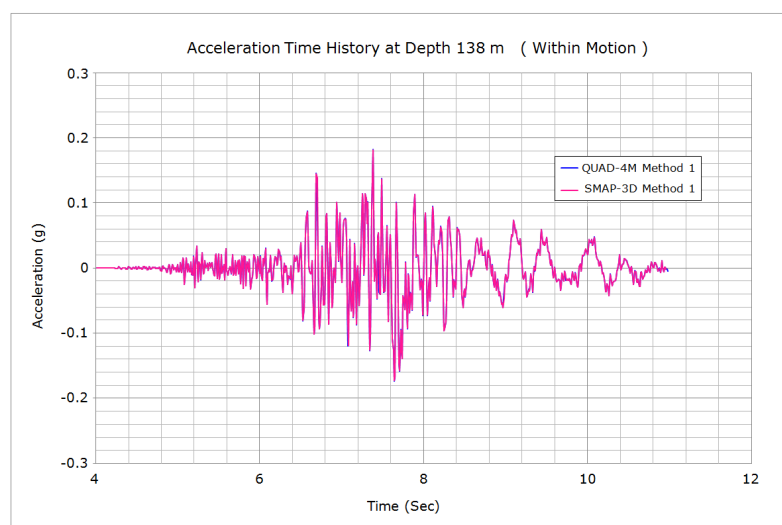
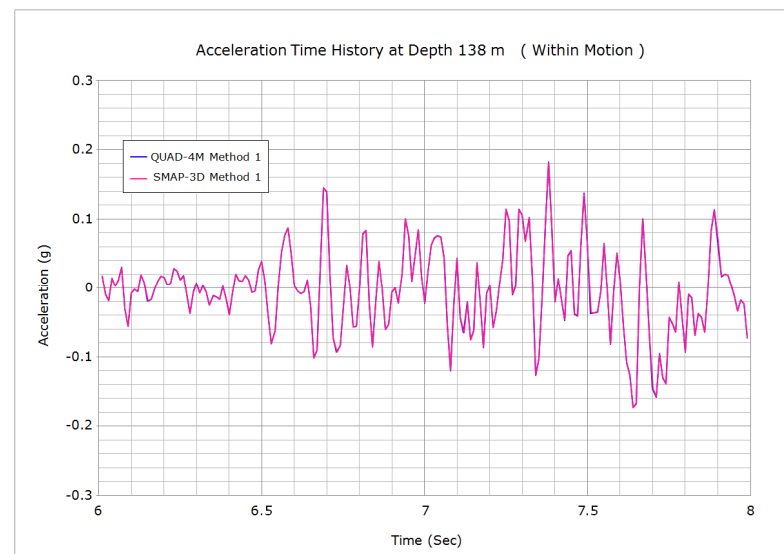


Figure 15. Acceleration time history at depth 138 m (within motion) which compare QUAD-4M to SMAP-3D.



**Figure 16.** Acceleration history at depth 138 m which compare QUAD-4M to SMAP-3D, between 6 and 8 s.

#### 4. Linear Frequency vs. Linear Time Domain Analysis

##### 4.1. General

In this section, SMAP-3D time domain solutions are compared to the exact closed-form frequency domain SHAKE91 solutions for the analysis of free-field responses subjected to vertically propagating shear waves caused by earthquake motions.

As described in the previous Section 3, finite element time domain solutions employ the frequency-dependent Rayleigh formulation to model material damping. Consequently, responses would be more damped at some frequencies and less damped at the other frequencies. On the other hand, the damping scheme in SHAKE91 is independent of frequency.

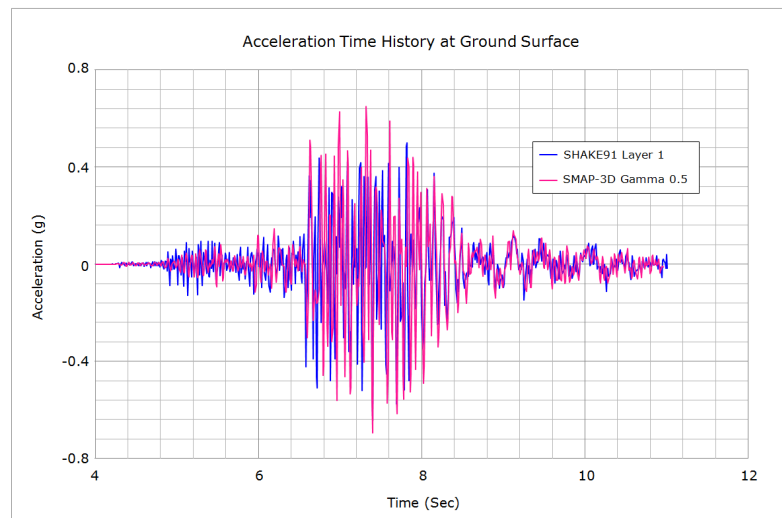
Both SHAKE91 and SMAP-3D solutions are presented separately in the previous Sections 2 and 3, respectively. In this section, one additional analysis is conducted for SMAP-3D using numerical damping in the Newmark  $\beta$  method with  $\gamma = 1$ . Obviously, such numerical damping will damp down the responses associated with high-frequency modes. However, it is often applied to obtain stable solutions when the material state changes abruptly due to brittle failure or joint separation during strong shaking dynamic motions.

##### 4.2. Analysis Results

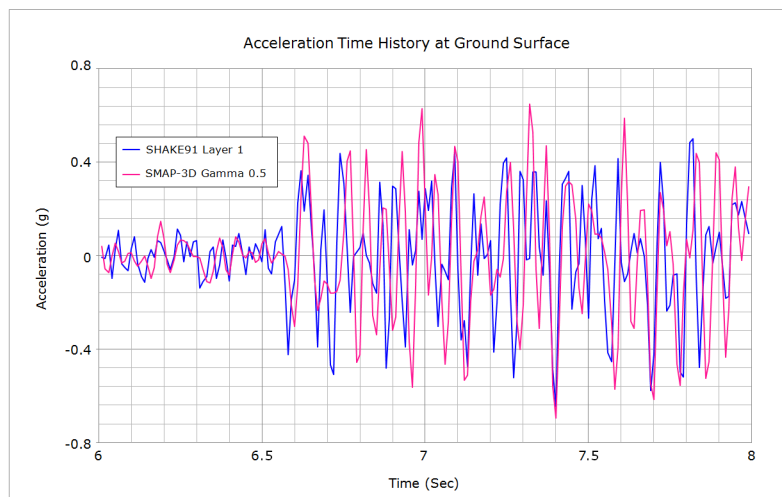
Figure 17 shows the acceleration time histories on the ground surface which compare the SMAP-3D with  $\gamma = 0.5$  to SHAKE91. Figure 18 shows the same comparison between  $t = 6$  and  $t = 8$  s. Compared to SHAKE91, SMAP-3D results show somewhat higher responses at the time when strong motions occur.

Figure 19 shows the acceleration time histories at a depth of 138 m which compares the SMAP-3D with  $\gamma = 0.5$  to SHAKE91. Figure 20 shows the same comparison between  $t = 6$  and  $t = 8$  s, where strong motions occur. SMAP-3D results at this depth show closer to SHAKE91 results than we see those comparisons on the ground surface. Note that this depth corresponds to the location of the silo mid height as shown in Figure 4.

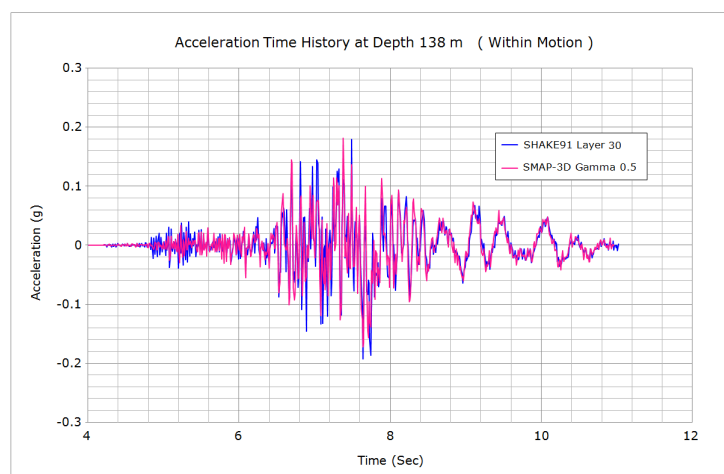
Figure 21 shows the acceleration time histories on the ground surface which compare the SMAP-3D with  $\gamma = 1$  to SHAKE91. Figure 22 shows the same comparison between  $t = 6$  and  $t = 8$  s. Compared to SHAKE91, SMAP-3D results show significantly damped responses in the time when strong motions occur.



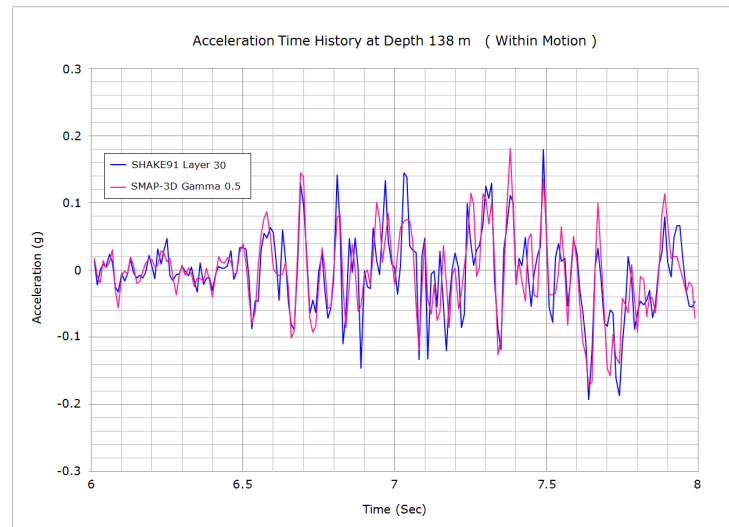
**Figure 17.** Acceleration time history on the ground surface which compare the SMAP-3D with  $\gamma = 0.5$  to SHAKE91.



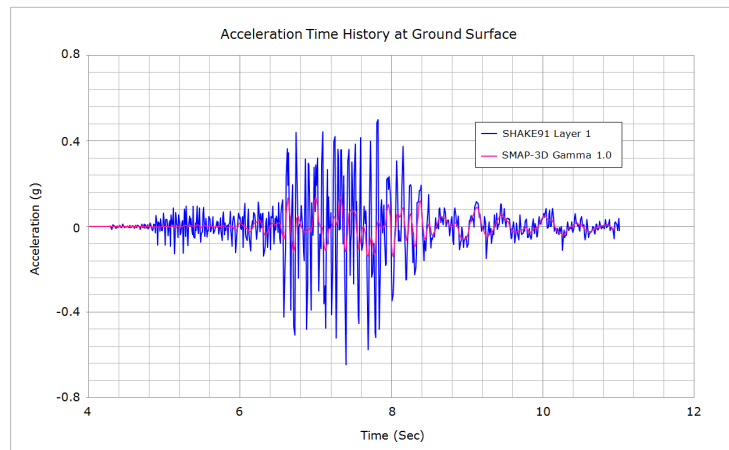
**Figure 18.** Acceleration history on the ground surface, between 6 and 8 s.



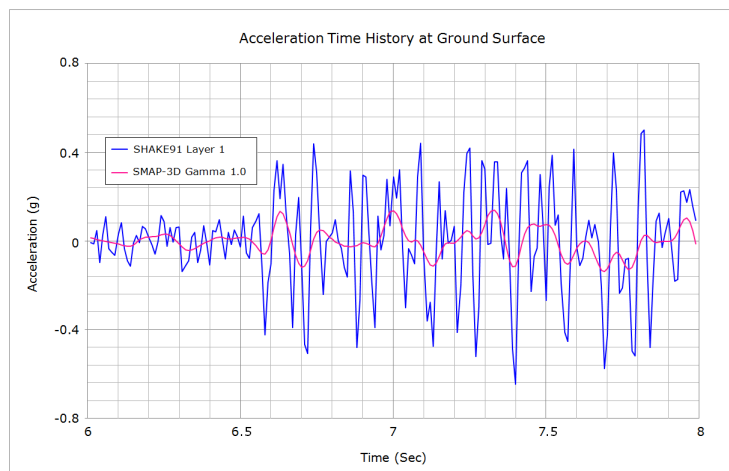
**Figure 19.** Acceleration time history at depth 138 m (within motion) which compares the SMAP-3D with  $\gamma = 0.5$  to SHAKE91.



**Figure 20.** Acceleration history at depth 138 m which compares the SMAP-3D with  $\gamma = 0.5$  to SHAKE91, between 6 and 8 s.



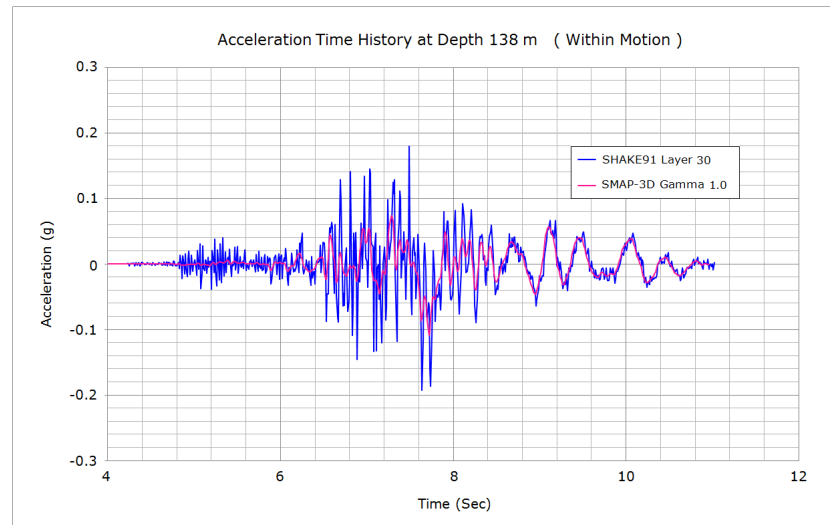
**Figure 21.** Acceleration time history on the ground surface which compare the SMAP-3D with  $\gamma = 1$  to SHAKE91.



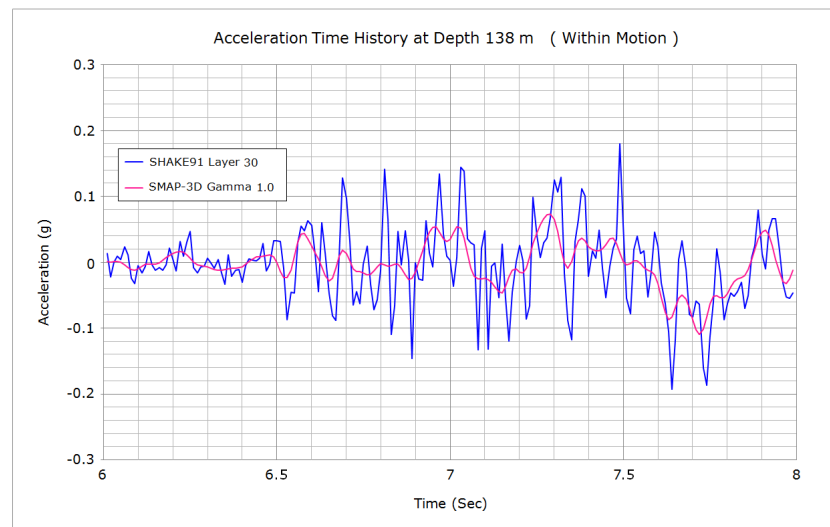
**Figure 22.** Acceleration history on the ground surface, between 6 and 8 s.

Figure 23 shows the acceleration time histories at a depth of 138 m which compare the SMAP-3D with  $\gamma = 1$  to SHAKE91. Figure 24 shows the same comparison between  $t = 6$

and  $t = 8$  s. Compared to SHAKE91, SMAP-3D results show moderately damped responses in the time when strong motions occur. Note that this depth corresponds to the location of the silo mid height as shown in Figure 4.



**Figure 23.** Acceleration time history at depth 138 m (within motion) which compare the SMAP-3D with  $\gamma = 1$  to SHAKE91.



**Figure 24.** Acceleration history at depth 138 m which compare the SMAP-3D with  $\gamma = 1$  to SHAKE91, between 6 and 8 s.

So far, all comparisons are based on the acceleration time histories. Now, we want to make some comparisons based on relative displacement and shear stress time histories.

Figure 25 shows the relative displacement time histories on the ground surface which compare the SMAP-3D with  $\gamma = 0.5$  and  $\gamma = 1$  to SHAKE91. Figure 26 shows the same comparison between  $t = 7$  and  $t = 9$  s. Compared to SHAKE91, SMAP-3D results are closer to SHAKE91 results than we see those comparisons for acceleration histories. It is also noticed that the effect of numerical damping is less significant in the relative displacements.

Figures 27 and 28 show the relative displacement time histories at the depth 138 m and on the bottom surface, respectively, which compare the SMAP-3D with  $\gamma = 0.5$  and  $\gamma = 1$  to SHAKE91. We can see the same trends as in the ground surface. Here, also, the numerical damping has a slight influence on the response of relative displacements.

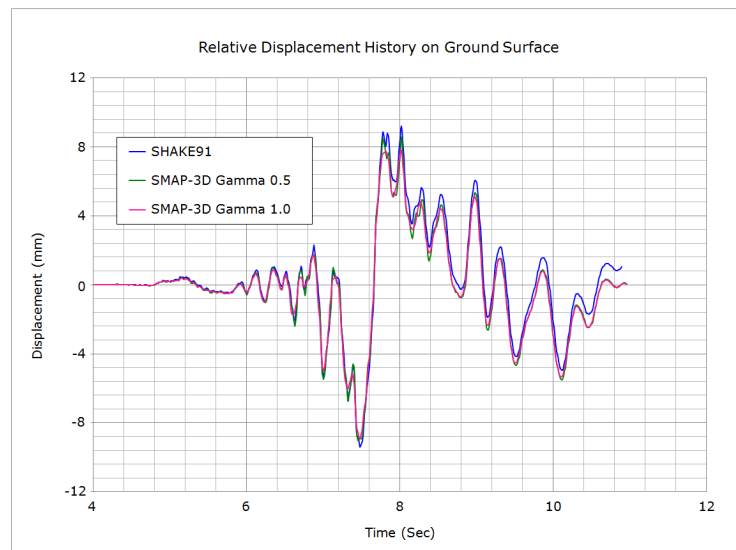


Figure 25. Relative displacement history on the ground surface.

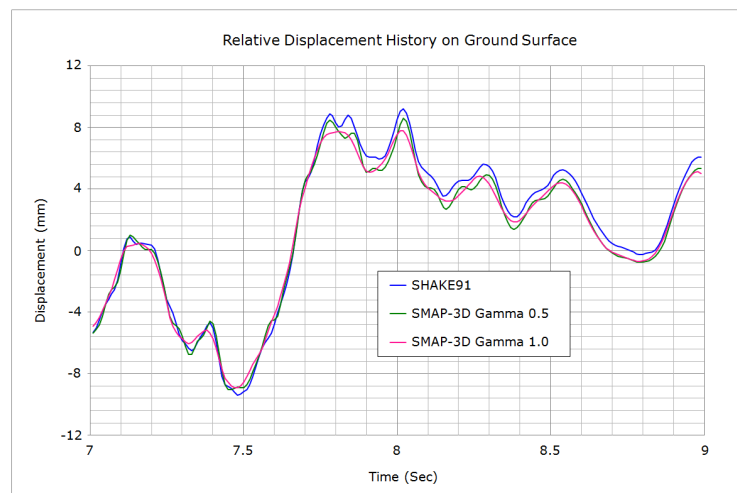


Figure 26. Relative displacement history on the ground surface, between 7 and 9 s.

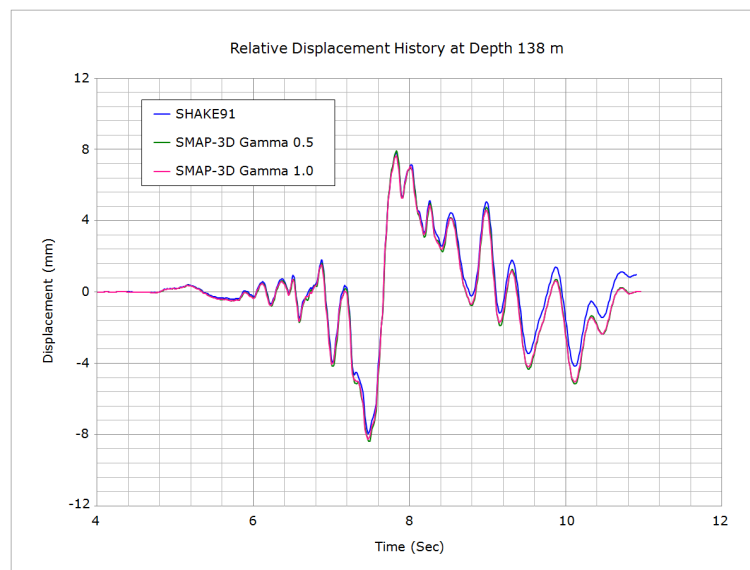


Figure 27. Relative displacement history at depth 138 m (within motion).

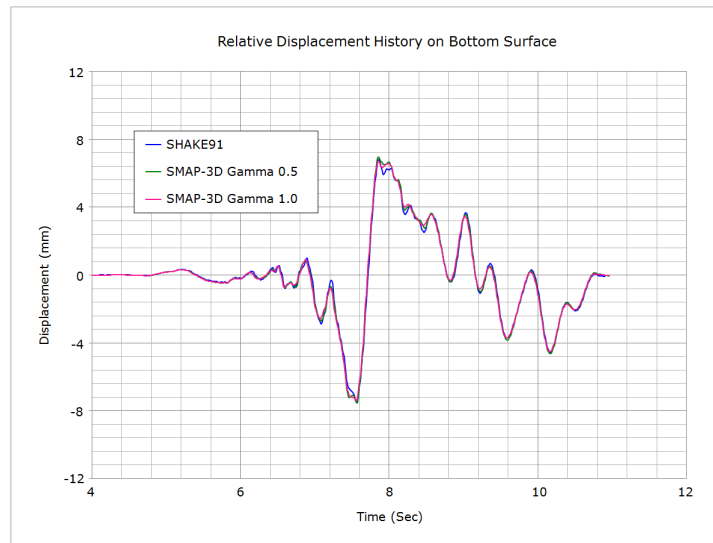


Figure 28. Relative displacement history on the bottom surface (within motion).

Figure 29 shows the shear stress time histories at a depth of 138 m which compares the SMAP-3D with  $\gamma = 1$  to SHAKE91. Figure 30 shows the same comparison between  $t = 6$  and  $t = 8$  s. SMAP-3D calculation with numerical damping of  $\gamma = 1$  predicts reasonably well SHAKE91 closed-form results. Note that this depth corresponds to the location of the silo mid height as shown in Figure 4.

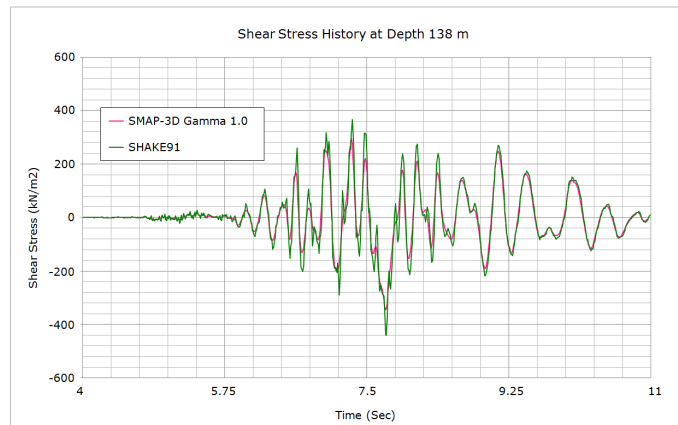


Figure 29. Shear stress history at depth 138 m.

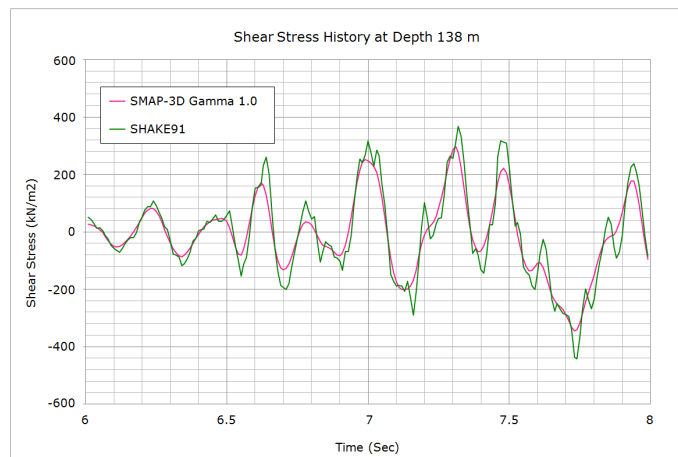


Figure 30. Shear stress history at depth 138 m, between 6 and 8 s.

## 5. Conclusions

Comparative studies between the frequency domain analysis and time domain analysis on free-field one-dimensional analysis are presented in this paper. Free-field one-dimensional analyses have been carried out considering the following.

- Closed-form solutions (SHAKE, SHAKE91, DEEPSOIL, etc.) in the frequency domain are available for one-dimensional shear wave propagation in the linearly viscous elastic system subjected to base accelerations.
- Numerical finite element solutions as the time domain analysis can be directly compared to such closed-form solutions in the free fields including lateral boundary so that we can assess the accuracy of numerical solutions.

The following conclusions arise from numerical studies presented in this paper.

- (1) Two computer programs (SHAKE91 and DEEPSOIL) are selected for the closed-form solutions in the frequency domain. The acceleration time histories on the ground surface which compare SHAKE91 to DEEPSOIL show almost identical responses in the time where strong motions occur. The acceleration time histories at the location of the silo mid-height show also almost identical responses in the time where strong motions occur.
- (2) One modal analysis (SRAP-1D) and two finite element computer programs (QUAD-4M, and SMAP-3D) are selected to perform the free-field analysis in the time domain. The acceleration time histories on the ground surface which compare the results of all three computer programs show almost identical responses in the time where strong motions occur. It also shows that Method 1, the conventional procedure, produces almost the same results as Method 2. The acceleration time histories at the location of the silo mid height which compare QUAD-4M to SMAP-3D show almost identical responses in the time where strong motions occur.
- (3) SMAP-3D time domain solutions are compared to the exact closed-form frequency domain SHAKE91 solutions for the analysis of free-field responses subjected to vertically propagating shear waves caused by earthquake motions. As a result of comparing SMAP-3D with  $\gamma = 0.5$  and SHAKE91 to the acceleration time histories on the ground surface, SMAP-3D results show somewhat higher responses in the time where strong motions occur. SMAP-3D results at the location of the silo mid height are closer to SHAKE91 results than we see in those comparisons on the ground surface.
- (4) Compared to SHAKE91, SMAP-3D with  $\gamma = 1.0$  results show significantly damped responses in the time where strong motions occur to the acceleration time histories on the ground surface. Compared to SHAKE91, SMAP-3D results show also moderately damped responses in the time where strong motions occur to the acceleration time histories at the location of the silo mid height.
- (5) For the relative displacement time histories on the ground surface, SMAP-3D with  $\gamma = 0.5$  and  $\gamma = 1$  results show closer to SHAKE91 results than we see in those comparisons for acceleration histories. It is also noticed that the effect of numerical damping is less significant in the relative displacements. Compared to SHAKE91, SMAP-3D with  $\gamma = 0.5$  and  $\gamma = 1$  results in the relative displacement time histories at the location of the silo mid height show the same trends as at the ground surface. Here, also, the numerical damping has a slight influence on the response of relative displacements.
- (6) SMAP-3D calculation with numerical damping of  $\gamma = 1$  to the shear stress time histories at the location of the silo mid height predicts reasonably well SHAKE91 closed-form results.

**Author Contributions:** Conceptualization, S.-H.K.; Methodology, K.-J.K.; Software, K.-J.K.; Formal analysis, K.-J.K.; Resources, S.-H.K.; Writing—original draft, K.-J.K.; Writing—review and editing, S.-H.K.; Funding acquisition, S.-H.K. All authors have read and agreed to the published version of the manuscript.

**Funding:** This work was partially supported by the “Radioactive Waste Management Program” of the Korea Institute of Energy Technology Evaluation and Planning (KETEP) granted financial resources from the Ministry of Trade, Industry and Energy, Republic of Korea (Project No. 20193210100040).

**Data Availability Statement:** The original contributions presented in this study are included in the article, further inquiries can be directed to the corresponding author.

**Acknowledgments:** We would like to thank the Korea Institute of Energy Technology Evaluation and Planning (KETEP) granted financial resources from the Ministry of Trade, Industry and Energy, Republic of Korea, for supporting research funding. We would also like to thank Jeong-Gon Ha of Korea Atomic Energy Research Institute for providing the earthquake data in Gyeongju Myeonggye-ri, Republic of Korea, for conducting this study.

**Conflicts of Interest:** Author Kwang-Jin Kim was employed by the company Comtec Research. The authors declare that the research was conducted in the absence of any commercial or financial relationships that could be construed as a potential conflict of interest.

## References

1. Aikas, T.; Anttila, P. Repositories for low- and intermediate-level radioactive wastes in Finland. *Rev. Eng. Geol.* **2008**, *19*, 67–71. [[CrossRef](#)]
2. KORAD. *Earth & Us*; Korea Radioactive Waste Agency: Gyeongju, Republic of Korea, 2018.
3. Shin, Y.; Lee, J. The status and experiences of LILW disposal facilities construction. *J. Korean Soc. Miner Energy Resour. Eng.* **2017**, *54*, 389–396. (In Korean) [[CrossRef](#)]
4. Kim, S.H.; Kim, K.J. Numerical parametric studies on the stress distribution in rocks around underground silo. *Appl. Sci.* **2022**, *12*, 1613. [[CrossRef](#)]
5. Park, J.B.; Jung, H.R.; Lee, E.Y.; Kim, C.L.; Kim, G.Y.; Kim, K.S.; Koh, Y.K.; Park, K.W.; Cheong, J.H.; Jeong, C.W.; et al. Wolsong low- and intermediate-level radioactive waste disposal center: Progress and challenges. *Nucl. Eng. Techno.* **2009**, *41*, 477–492. [[CrossRef](#)]
6. Bang, J.H.; Park, J.H.; Jung, K.I. Development of two-dimensional near-field integrated performance assessment model for near-surface LILW disposal. *J. Nucl. Fuel Cycle Waste Tech.* **2014**, *12*, 315–334. [[CrossRef](#)]
7. Jung, K.I.; Kim, J.H.; Kwon, M.J.; Jeong, M.S.; Hong, S.W.; Park, J.B. Comprehensive development plans for the low- and intermediate-level radioactive waste disposal facility in Korea and preliminary safety assessment. *J. Nucl. Fuel Cycle Waste Tech.* **2016**, *14*, 385–410. [[CrossRef](#)]
8. Kim, K.H.; Ree, J.H.; Kim, Y.H.; Kim, S.S.; Kang, S.Y.; Seo, W.S. Assessing whether the 2017 Mw 5.4 Pohang earthquake in South Korea was an induced event. *Science* **2018**, *360*, 1007–1009. [[CrossRef](#)] [[PubMed](#)]
9. Jin, K.; Lee, J.; Lee, K.; Kyung, J.B.; Kim, Y.S. Earthquake damage and related factors associated with the 2016 ML=5.8 Gyeongju earthquake, southeast Korea. *Geosci. J.* **2020**, *24*, 141–157. [[CrossRef](#)]
10. Kim, M.K.; Choi, I.K.; Jeong, J. Development of a seismic risk assessment system for low and intermediate level radioactive waste repository—Current status of year 1 research. In Proceedings of the WM2011 Conference, Phoenix, AZ, USA, 3 March 2011.
11. Byen, H.; Jeong, G.Y.; Park, J. Structural stability analysis of waste packages containing low- and intermediate-level radioactive waste in a silo-type repository. *Nucl. Eng. Techno.* **2021**, *53*, 1524–1533. [[CrossRef](#)]
12. Byeon, H.; Park, J.; Kim, B. Seismic analysis of waste packages stacked in radioactive waste disposal silos. *Tunn. Undergr. Sp. Tech.* **2023**, *140*, 105287. [[CrossRef](#)]
13. Mansour, S.; Pieraccini, L.; Foti, D.; Gasparini, G.; Trombetti, T.; Silvestri, S. Comprehensive review on the dynamic and seismic behavior of flat-bottom cylindrical silos filled with granular material. *Front. Built Environ.* **2022**, *7*, 2021. [[CrossRef](#)]
14. Foti, D.; Trombetti, T.; Silvestri, S.; Chiacchio, L.; Ivorra, S.; Taylor, C.; Dietz, M. Analysis of the dynamic behavior of squat silos containing grain-like material subjected to shaking table tests—ASESGRAM final report. In *Experimental Research in Earthquake Engineering*; Taucer, F., Apostolska, R., Eds.; Springer: Cham, Switzerland, 2015; Volume 35. [[CrossRef](#)]
15. Mansour, S.; Silvestri, S.; Sadowski, A.J. The ‘miniature silo’ test; A simple experimental setup to estimate the effective friction coefficient between the granular solid and a horizontally-corrugated cylindrical metal silo wall. *Powder Technol.* **2022**, *399*, 117212. [[CrossRef](#)]
16. Dongangun, A.; Karaca, Z.; Durmus, A.; Sezen, H. Cause of damage and failures in silo structures. *J. Perform. Constr. Facil.* **2009**, *23*, 65–71. [[CrossRef](#)]
17. Younan, A.H.; Veletsos, A.S. Dynamics of silos-containing tanks. I: Rigid tanks. *J. Struct. Eng.* **1998**, *124*, 52–61. [[CrossRef](#)]
18. Kim, S.H.; Kim, K.J. Finite element formulations for free field one-dimensional shear wave propagation. *Earthquakes Struct.* **2024**, *26*, 163–174. [[CrossRef](#)]
19. Kim, S.H.; Kim, K.J. Numerical Study of Structural Behavior of Underground Silo Structures for Low-and-Intermediate-level Radioactive Waste Disposal Facility. *J. Comput. Struct. Eng. Inst. Korea* **2022**, *35*, 183–190. (In Korean) [[CrossRef](#)]

20. Idriss, I.M.; Sun, J.I. *User's Manual for SHAKE91: A Computer Program for Conducting Equivalent Linear Seismic Response Analyses of Horizontally Layered Soil Deposits*; Center for Geotechnical Modeling, Department of Civil & Environmental Engineering, University of California: Davis, CA, USA, 1992.
21. Hashash, Y.M.A.; Musgrove, M.I.; Harmon, J.A.; Ilhan, O.; Xing, G.; Numanoglu, O.; Groholski, D.R.; Phillips, C.A.; Park, D. *DEEPSOIL 7, User Manual*; Board of Trustees of University of Illinois at Urbana-Champaign: Urbana, IL, USA, 2020.
22. Idriss, I.M.; Seed, H.B. *Response of Horizontal Soil Layers During Earthquakes*; Research Report; Soil Mechanics and Bituminous Materials Laboratory, University of California: Berkeley, CA, USA, 1967.
23. Hudson, M.; Idriss, I.M.; Beikae, M. *User's Manual for QUAD4M: A Computer Program to Evaluate the Seismic Response of Soil Structures Using Finite Element Procedures and Incorporating a Compliant Base*; University of California: Davis, CA, USA, 1994.
24. Comtec Research. *SMAP-3D; Structure Medium Analysis Program, User's Manual Version 7.03*; Comtec Research: Seattle, WA, USA, 2020.
25. Schnabel, P.B.; Lysmer, J.; Seed, H.B. *SHAKE—A Computer Program for Earthquake Response Analysis of Horizontal Layered Sites*; Report. No. EERC 71-12; Earthquake Engineering Research Center: Berkeley, CA, USA, 1972.
26. Ordonez, G.A. *SHAKE2000: A Computer Program for the 1-D Analysis of Geotechnical Earthquake Engineering Problems*; Geomotion, LLC: Lacey, WA, USA, 2012.
27. McCallen, D.B. *SPECTRA: A Subroutine for Response Spectra Generation*; Lawrence Berkeley National Laboratory: Berkeley, CA, USA, 1991.
28. Millen, M. EQSIG; A Python Package for Seismic Signal Processing v1.2.10; Pypi. Python Package Repository. 2019. Available online: <https://pypi.org/project/eqsig/> (accessed on 19 April 2021).
29. Jeong, S.H.; Lee, K.H.; Jang, W.S. *PRISM; A Program for seismic response analysis of SDOF system, Version 2.0.0*; Department of Architectural Engineering, INHA University: Incheon, Republic of Korea, 2010.
30. Rayleigh, J.; Lindsay, R. *The Theory of Sound*; Dover Publications, Inc.: Dover, DE, USA, 1945.
31. Lai, C.G.; Rix, G.J. *Simultaneous Inversion of Rayleigh Phase Velocity and Attenuation for Near-Surface Site Characterization*; Report No. GIT-CEE/GEO-98-2; School of Civil and Environmental Engineering, Georgia Institute of Technology: Atlanta, GA, USA, 1988.
32. Hudson, M. Behavior of Slopes and Earth Dams during Earthquakes. Ph.D. Thesis, University of California, Davis, DE, USA, 1994.

**Disclaimer/Publisher's Note:** The statements, opinions and data contained in all publications are solely those of the individual author(s) and contributor(s) and not of MDPI and/or the editor(s). MDPI and/or the editor(s) disclaim responsibility for any injury to people or property resulting from any ideas, methods, instructions or products referred to in the content.